Structure of the Erythrocyte Membrane Skeleton as Observed by Atomic Force Microscopy

Minoru Takeuchi,* Hiroshi Miyamoto,# Yasushi Sako,§ Hideo Komizu,# and Akihiro Kusumi§

*Department of Life Sciences, Graduate School of Arts and Sciences, The University of Tokyo, Meguro-ku, Tokyo 153; #Biosignaling Department, National Institute of Bioscience and Human-Technology, 1-1 Higashi, Tsukuba 305; and §Department of Biological Science, Graduate School of Science, Nagoya University, Chikusa-ku, Nagoya 464-8602, Japan

ABSTRACT The structure of the membrane skeleton on the cytoplasmic surface of the erythrocyte plasma membrane was observed in dried human erythrocyte ghosts by atomic force microscopy (AFM), taking advantage of its high sensitivity to small height variations in surfaces. The majority of the membrane skeleton can be imaged, even on the extracellular surface of the membrane. Various fixation and drying methods were examined for preparation of ghost membrane samples for AFM observation, and it was found that freeze-drying (freezing by rapid immersion in a cryogen) of unfixed specimens was a fast and simple way to obtain consistently good results for observation without removing the membrane or extending the membrane skeleton. Observation of the membrane skeleton at the external surface of the cell was possible mainly because the bilayer portion of the membrane sank into the cell during the drying process. The average mesh size of the spectrin network observed at the extracellular and cytoplasmic surfaces of the plasma membrane was 4800 and 3000 nm^2, respectively, which indicates that spectrin forms a three-dimensionally folded meshwork, and that 80% of spectrin can be observed at the extracellular surface of the plasma membrane.

INTRODUCTION

Many functions of the plasma membrane involve its long-range molecular and structural organization. For example, the internalization of receptors and the adhesion of cells both require the recruitment and assembly of intra- and peripheral-membrane proteins over long distances in the plasma membrane (Jacobson et al., 1995; Kusumi and Sako, 1996). Polarization of epithelial cells, changes in cell shapes, and crawling of cells all require the mechanical regulation of the long-range structure of the plasma membrane (Hammerton et al., 1991; Tsukita et al., 1992; Sheets et al., 1995; Tsuji et al., manuscript submitted for publication). Such long-range organizations require more than a simple membrane in which integral membrane proteins are floating in a sea of excess lipids, as proposed by the fluid mosaic model. Accumulating data show that the membrane-associated portion of the cytoskeleton, or the membrane skeleton, is involved in the organization and mechanical regulation of the plasma membrane (Bennett, 1990; Luna and Hitt, 1992; Bennett and Gilligan, 1993; Hitt and Luna, 1994; Boal, 1994; Boal and Boey, 1995; Sako and Kusumi, 1994, 1995; Kusumi and Sako, 1996). Further investigation of the interaction between the bilayer part of the membrane and the cytoskeleton/membrane skeleton is needed to understand the long-range structural basis of the functions of the plasma membrane.

Received for publication 27 March 1997 and in final form 8 February 1998.

Address reprint requests to Dr. Akihiro Kusumi, Department of Biological Science, Graduate School of Science, Nagoya University, Chikusa-ku, Nagoya 464-8602, Japan. Tel.: 011-81-52-789-2969; Fax: 011-81-52-789-2968; E-mail: akusumi@bio.nagoya-u.ac.jp.

0006-3495/98/05/2171/13 $2.00

Henderson et al. (1992) and Chang et al. (1993) showed that actin filaments and other cytoskeletons in living cells can be observed at the extracellular surface of the plasma membrane, without any staining, by atomic force microscopy (AFM). In this technique, a needle with a sharp tip (radius of curvature 10–50 nm) is scanned over the cell surface at a pressing force on the order of 0.1–10 nN, and the height of the needle is recorded at each position, thus generating an image of the terrain of the cell surface and/or the underlying structure of the (soft) cell surface. Because the plasma membrane is soft, the needle either presses down on the membrane or penetrates the membrane and forms images of the harder structures inside the cell. Therefore, these reports raise the possibility that structures near the plasma membrane, such as the membrane skeleton, can be visualized on the extracellular surface of the plasma membrane. The goal of the present research was to examine this possibility and to develop an AFM method for observing the membrane-skeleton/cytoskeleton at the extracellular surface of the cell. A major advantage of AFM as compared with other microscopic techniques is that it provides better resolution than optical microscopy and yet allows the observation of living cells, which is impossible with an electron microscope. AFM observations of the cytoskeleton/membrane skeleton have also been made by Pietrasanta et al. (1994), Lal et al. (1995), and Horber et al. (1995).

As an initial step in AFM studies on the membrane skeleton structure, we chose to examine human red blood cells, because they contain a well-developed membrane skeleton network, their membrane skeleton is biochemically better characterized than those of other cells, and the expanded structure of the membrane skeleton meshwork has been studied by electron microscopy. Previous studies using transmission electron microscopy (EM) have revealed var-

ious important morphological features of the meshwork (Sheetz and Sawyer, 1978; Timme, 1981; Byers and Branton, 1985; Shen et al., 1986; Liu et al., 1987; Ursitti et al., 1991; Ursitti and Wade, 1993) and provide the basis for the present research. However, in these studies, the membrane skeleton was separated from the plasma membrane by isolation with Triton, except in the study by Ursitti et al. (1991). To observe the membrane skeleton network, it was often further artificially spread by low pH or low ionic strength. Although this method allowed for close inspection of the interaction of major proteins in the erythrocyte membrane skeleton (Byers and Branton, 1985; Shen et al., 1986; Liu et al., 1987), the intact structure of the membrane skeleton was lost during this process.

Our knowledge regarding how the erythrocyte membrane skeleton network is organized in situ is very limited. This in turn limits our understanding of the structural basis for the elasticity and resilience of erythrocytes in circulation (Evans, 1989; Vertessy and Steck, 1989) and of the loss of these properties in pathological states (reviewed in Mohandas and Chasis, 1993). The erythrocyte's membrane-associated skeleton without detergent solubilization of the membrane has been visualized by several methods, including scanning electron microscopy (Hainfeld and Steck, 1977), thin-section electron microscopy (Tsukita et al., 1980), and electron microscopy after freeze-etching and platinum replication (Nermut, 1981; Ursitti et al., 1991; also see figure 2 *a* in the review by Coleman et al. (1989), which was taken by Dr. J. Heuser of Washington University). These studies showed that the membrane skeleton is a dense, complex, three-dimensional network of filaments that is difficult to analyze in detail (Weinstein et al., 1986). Thus the second goal of this work was to establish a method for studying the membrane skeleton network of human erythrocyte by AFM, without removing the plasma membrane by detergent treatment and without extending or staining the membrane skeleton. Erythrocytes have been observed by AFM (Butt et al., 1990; Gould et al., 1990; Han et al., 1995; Zhang et al., 1996), but the structure of the membrane skeleton as observed by AFM has not been described. Isolated spectrin has also been observed by AFM (Almqvist et al., 1994).

The major constituent of the membrane skeleton is spectrin dimers, flexible units of the network that are 100 nm long in the extended form (Shotton et al., 1979). Spectrin dimers associate head-to-head to form tetramers (Liu et al., 1984; Beaven et al., 1985) that are linked together into a two-dimensional net-like meshwork by junctional complexes, which are composed of short (~33 nm) actin filaments consisting of 8–13 actin monomers, band 4.1, glycophorin C (a transmembrane protein), and several other minor protein components (Ohanian et al., 1984; Byers and Branton, 1985; Shen et al., 1986; reviewed by Gilligan and Bennett, 1993). A two-dimensional spectrin meshwork formed by interactions on both ends of spectrin dimers covers the entire cytoplasmic surface of the erythrocyte membrane (Lux, 1979; Marchesi, 1985).

Initially we attempted to observe intact erythrocytes, ghosts, or fixed ghosts in an aqueous buffer, but it was difficult to obtain high-resolution images of the membrane skeleton in the aqueous medium. This may be because the erythrocyte membrane skeleton is thermally fluctuating and/or is deformed with the force applied by the AFM probe.

Therefore, in the present study, we concentrated our effort on observing the membrane skeleton structure of dried ghosts. A variety of fixation and drying methods were examined to optimize the preparation of ghost samples for AFM observation. Observations were made on both the extracellular and the cytoplasmic surfaces of the plasma membrane.

MATERIALS AND METHODS

Reagents

Reagents were obtained from the following sources: liquid cryogen HFC-134a was from Nisshin EM (Tokyo, Japan); alcian blue was from Nacalai (Kyoto, Japan); 10-nm colloidal gold was from British BioCell (Cardiff, Wales); rabbit anti-spectrin antibodies, bovine serum albumin (BSA), and Ficoll type 400 were from Sigma (St. Louis, MO); and cholesterol was from Boehringer Mannheim (Indianapolis, IN). All other reagents were obtained from Wako (Osaka, Japan).

Preparation of ghosts

Erythrocyte ghosts were prepared as described by Tsuji et al. (1988). Briefly, 10 ml blood was obtained from one of the authors (nonsmoker, type AB, Rh+), using EDTA as anticoagulant. All of the following steps (before the drying process) were conducted at 0°C. Erythrocytes were washed four times in 140 mM NaCl, 5 mM Na_3PO_4/Na_2HPO_4, and 20 μM phenylmethylsulfonylfluoride (pH 8.0) by centrifugation at 1500 $\times$ *g* for 10 min. The supernatant and the white fluffy coat on the pellet surface were discarded. Erythrocytes were then lysed by incubating in 5 mM Na_3PO_4/Na_2HPO_4 (pH 8.0, 5P8) on ice for 30 min, and washed five to seven times by centrifugation at 20,000 $\times$ *g* for 20 min at 0°C until the ghost pellet became white. The washing buffer contained 10 mM NaCl (5P8–10). In the presence of 10 mM NaCl, the membrane skeleton tends to be more stable. The loose pellet was placed on a coverslip and incubated for 10 min, and then the unbound ghost was washed away with 5P8–10. In several cases, the coverslips were coated with alcian blue, which is positively charged (Sommer, 1977; Rutter and Hohenberg, 1991).

Lysis-squirting of ghosts

When the cytoplasmic surface of the ghost membrane had to be exposed for observation from inside the cell, a method of lysis-squirting was employed (Clarke et al., 1975; Nermut, 1981). After ghosts were adsorbed on the surface of a coverslip, a fast stream of 5P8–10 was applied to the ghosts at an oblique angle, using a syringe with a 25-gauge needle, which sheared away the upper membrane, exposing the cytoplasmic surface of the bottom membrane.

Fixation

When the ghosts were fixed, ghosts adsorbed on the surface of a coverslip were incubated with 2% glutaraldehyde in 5P8–10 at 4°C for 30 min. Unreacted glutaraldehyde was removed by washing in 5P8–10. In several

cases, the ghosts were further fixed with osmium tetroxide (0.005–0.5%) in 5P8–10 for 30 min.

Drying

The following four drying methods were compared: 1) rapid-freeze/freeze-drying from water without fixation (Costello, 1980; Elder et al., 1982), 2) air-drying from water with or without fixation, 3) freeze-drying in *t*-butyl alcohol (Akahori et al., 1988; Inoue and Osatake, 1988), and 4) critical-point drying.

Rapid freezing in aqueous solutions was carried out by quickly immersing the coverslips in the liquid cryogen HFC134a (1,1,1,2-tetrafluoroethane) at −101°C (liquid/solid phase transition temperature). Just before the sample was frozen, the coverslip with attached ghosts was rinsed in distilled water for several seconds to remove salts. The frozen samples were dried at −85°C and rewarmed to room temperature under vacuum. For air drying, after the coverslip was briefly rinsed in distilled water, excess water was thoroughly and quickly removed, and then the specimen was placed near the opening of a laminar flow chamber. The drying took place within 3–10 min under these conditions, as observed by optical microscopy.

Freeze-drying in *t*-butyl alcohol was carried out as described by Inoue and his colleagues (Inoue and Osatake, 1988; Inoue et al., 1989). Critical-point drying was carried out with an Eiko DX-1 (Mito, Japan). For these drying procedures, ghosts were first fixed with 2% glutaraldehyde and postfixed with 0.5% osmium tetroxide. In several specific cases in which delipidation was intended, osmium fixation was omitted. Treatment with osmium tetroxide cross-links unsaturated acyl chains of phospholipids. This would make the membrane harder and more resistant to the forces exerted on the membrane during dehydration, in addition to making the membrane resistant to lipid extraction in the organic solvents used in some of the dehydration processes. For freeze-drying in *t*-butyl alcohol, water was first replaced with an ethanol/water solution with gradual increases in ethanol, and finally with pure ethanol, and then ethanol was replaced with a *t*-butyl alcohol/ethanol solution with gradual increases in *t*-butyl alcohol, and finally with pure *t*-butyl alcohol (melting temperature 25.6°C). The

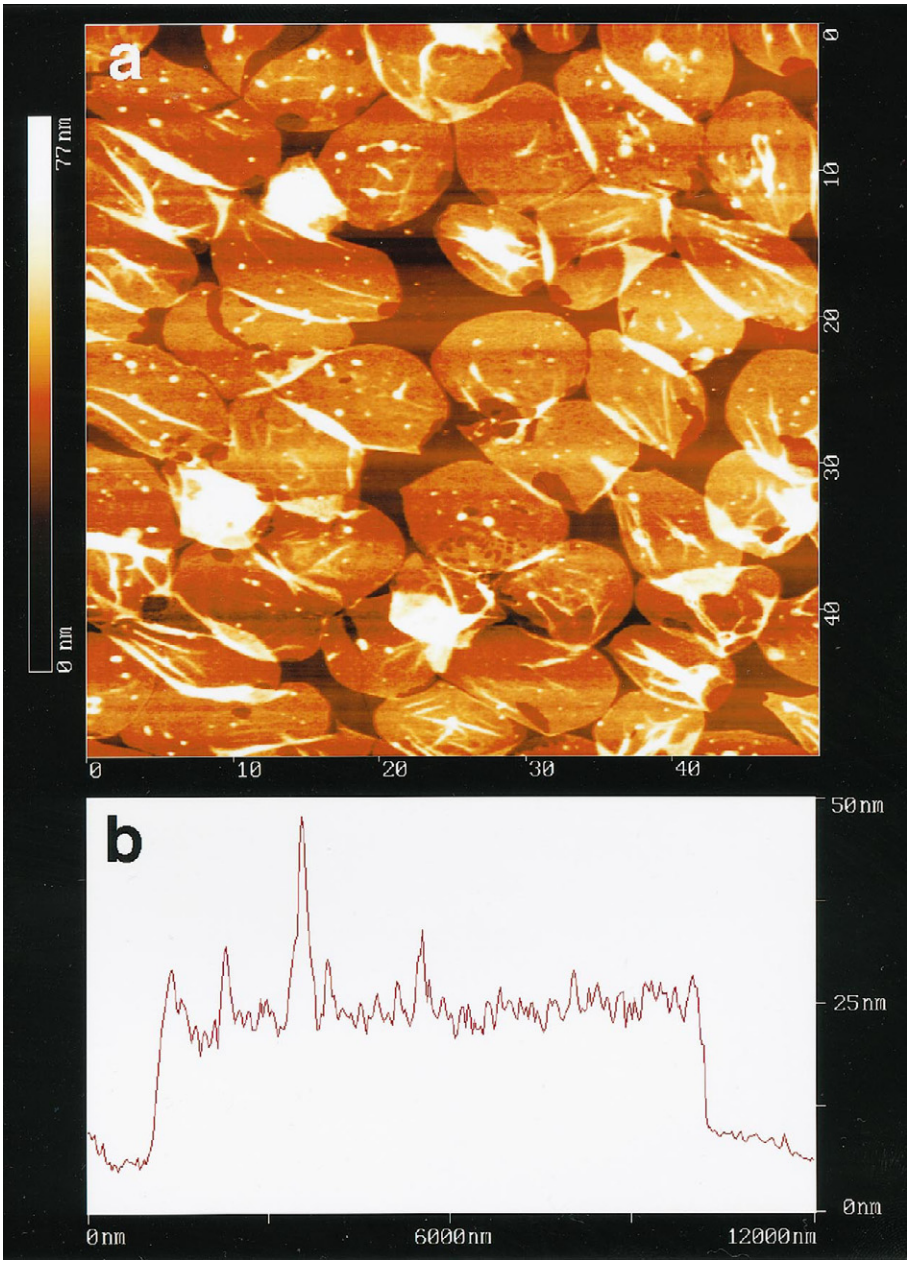

FIGURE 1 (*a*) An AFM image of rapidly frozen/freeze-dried unfixed ghosts on a coverslip at a low magnification. The surface of the coverslip is almost entirely covered with ghosts. Scales along the side of the image are in μm. (*b*) A representative surface contour along a line in an image of a single ghost. Note that the height in this profile is magnified 140 times more than the lateral dimensions (scale, nm).

sample was then frozen on a metal block that had been precooled to −85°C and then dried under vacuum at −10°C. For critical-point drying, the solvent for dehydration was replaced with ethanol.

Conjugation of anti-spectrin antibodies to gold particles and labeling of ghosts

Antibodies were adsorbed on colloidal gold particles 10 nm in diameter as described by Leunissen and De Mey (1989). A suspension of colloidal gold particles (2 ml, 0.01% w/v 10 nm-ϕ colloidal gold, pH adjusted to 9.4) was mixed with 100 μl of 1 mg/ml IgG fraction from rabbit anti-human spectrin serum or control serum. After incubation on ice for 1 h, 230 μl of 10% (w/v) BSA (pH 8.0) was added to the suspension, and the mixture was further incubated for 1 h. The suspension was centrifuged at 15,000 × g for 90 min, and the pellet was resuspended in 5P8–10 containing 1% BSA. The excess antibodies were removed by repeating centrifugation and resuspension in the same solution two more times. The conjugates were finally resuspended in 1 ml of 5P8–10 containing 1% BSA, filtered with 0.22-μm Millipore filters, and stored at 4°C.

To label ghosts with colloidal gold coated with anti-spectrin IgG, 0.3 ml antibody-conjugated gold solution was added to 100 μl ghost pellet, and the pellet was resuspended. After incubating on ice for 30 min, the ghosts were washed in 5P8–10 by five cycles of centrifugation and resuspension.

AFM observations

The coverslip was mounted on an AFM stage (scan area of 20 × 20 or 150 × 150 μm), and the ghosts were observed with an SPI 3700 AFM (Seiko Instruments, Chiba, Japan). Cantilevers with electron-beam-deposited tips with a tip radius of 10 nm and a spring constant of 0.12 N/m (HART probe; Materials Analytical Services, Raleigh, NC) were used. Observation was carried out in air at room temperature. The nominal applied force was ~3 nN. The scan speed of the tip was 10 μm/s or less. Distributions of mesh sizes observed from outside and inside the cell by AFM were evaluated with National Institutes of Health Image 1.45 software on a Macintosh personal computer. Three images of 1 μm^2 were randomly selected for each case, the network structure was extracted and skeletalized, and the area of each mesh was measured.

RESULTS AND DISCUSSION

Meshwork structure observed on the extracellular surface of the plasma membrane by AFM

In AFM, a needle with a sharp tip (radius of curvature is 10–50 nm) is scanned over the specimen surface at a pressing force of 0.1–10 nN, and the height of the needle (the feedback signal necessary to keep the force constant) is recorded at each position, thus generating an image of the surface terrain. Fig. 1 *a* shows an AFM image of freeze-dried ghosts (unfixed) on a coverslip. The ghosts were rapidly frozen by immersion in the liquid cryogen 1,1,2,2-tetrafluoroethane at −101°C. The surface of the coverslip is almost entirely covered with the ghosts. Many ghosts showed several sierras on the surface. However, the ghosts are 7–10 μm in diameter, showing that there is little lateral shrinkage of ghosts.

Fig. 1 *b* shows a representative surface contour of a ghost. Note that the vertical dimension in this profile is magnified 140 times more than the lateral dimensions. On average, the surface of the ghost lies ~14–18 nm above the coverslip, indicating shrinkage of the ghost in the direction normal to the coverglass surface. Formation of sierras is probably due

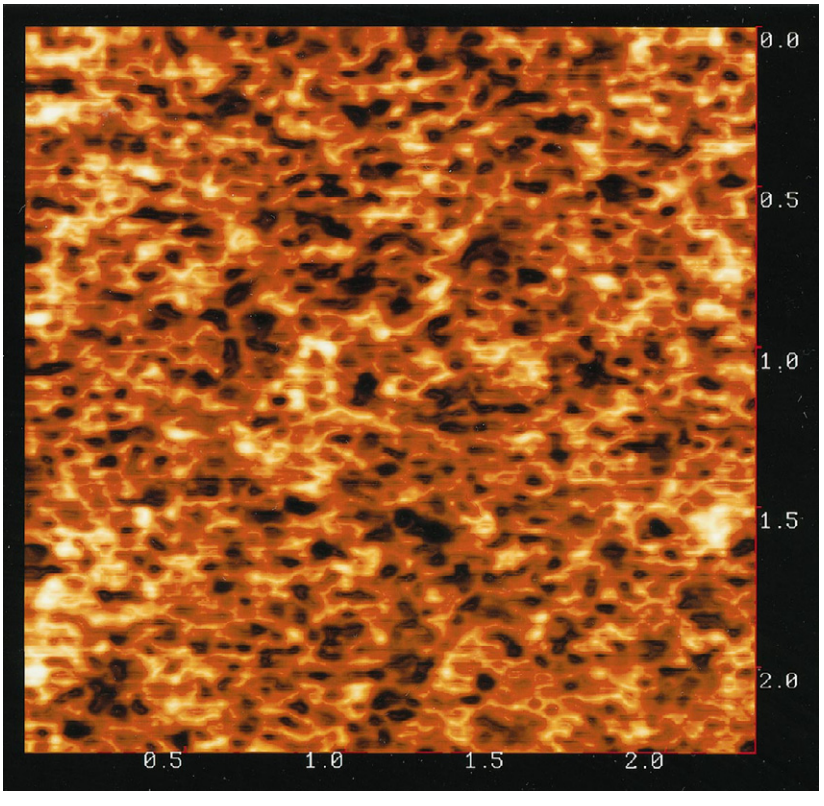

FIGURE 2 A representative high-magnification AFM image of a ghost as observed on the extracellular surface of the plasma membrane. The ghost was rapidly frozen/freeze-dried (unfixed). This image was generated by superposition of a height image and an illuminated image, using a light source placed at a 1 o'clock position, 70° above with respect to the surface. Scales are in μm.

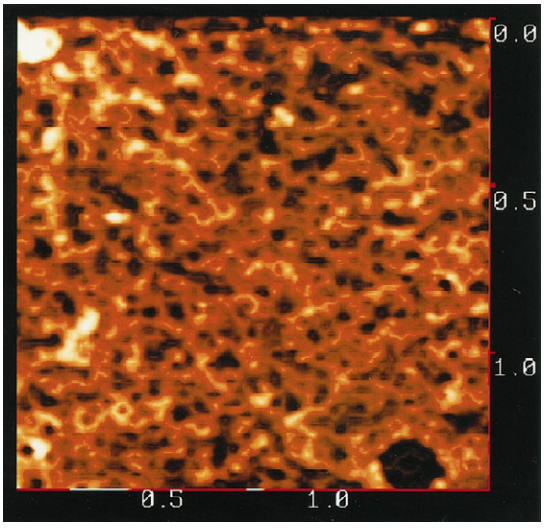

FIGURE 3 A representative AFM image of a carbon-coated (3 nm thick) ghost as observed on the extracellular surface of the plasma membrane. The unfixed ghost was rapidly frozen/freeze-dried and carbon-coated without rewarming under vacuum. The image was processed as described in Fig. 2. Scales are in μm.

to this shrinkage in the normal direction. (The peak near the left end is the cross section of a sierra.)

A representative AFM image of a ghost at a greater magnification is shown in Fig. 2. A dense network is clearly observed from outside the ghost by scanning the AFM tip over the cell. This resolution of the network was achieved only when electron-beam-deposited tips with a tip radius of 10 nm were used (100–250 nm long, HART probe; cf. Materials and Methods). The pressure applied with these sharp, high-aspect ratio tips could be significantly higher than that applied with a standard silicon nitride tip. However, because observed images are practically the same, even after the same area is scanned with these tips many times (more than 10 times), the tip pressure was not likely permanently change the sample. In addition, as shown later, the ghost sample coated with a 2- or 3-nm-thick carbon layer gave images similar to those of noncoated samples.

The spectrin network may be visualized through the membrane, which is only 4 nm thick. The next section gives data to show that this network indeed represents the spectrin network.

Dehydration of the membrane bilayer may induce the network structure such as those seen in Fig. 2. Using liposomes, it has been shown that after dehydration, the integrity of the bilayer is basically kept, and no structures like those detected here in the ghost membrane were observed (Bradow et al., 1993).

Partial rehydration of dried samples due to partitioning of atmospheric water into membranes under ambient conditions, which occurs when the samples are brought to ambient conditions after freeze-drying and rewarming to room temperature under vacuum, could also cause structural changes of the membrane. This might result in the images like those shown in Figs. 1 and 2. To examine the effect of rehydration, frozen samples were freeze-dried, and the surface structure was strengthened by carbon-coating (2–3 nm thick, either before or after the specimens were rewarmed under vacuum; all processing was carried out without breaking vacuum), and then the carbon-coated samples were observed by AFM. A typical image of a ghost carbon-coated before rewarming (under vacuum) and rehydration is shown in Fig. 3. Comparing the carbon-coated ghost in Fig. 3 with the uncoated ghost in Fig. 2, it is concluded that the carbon-

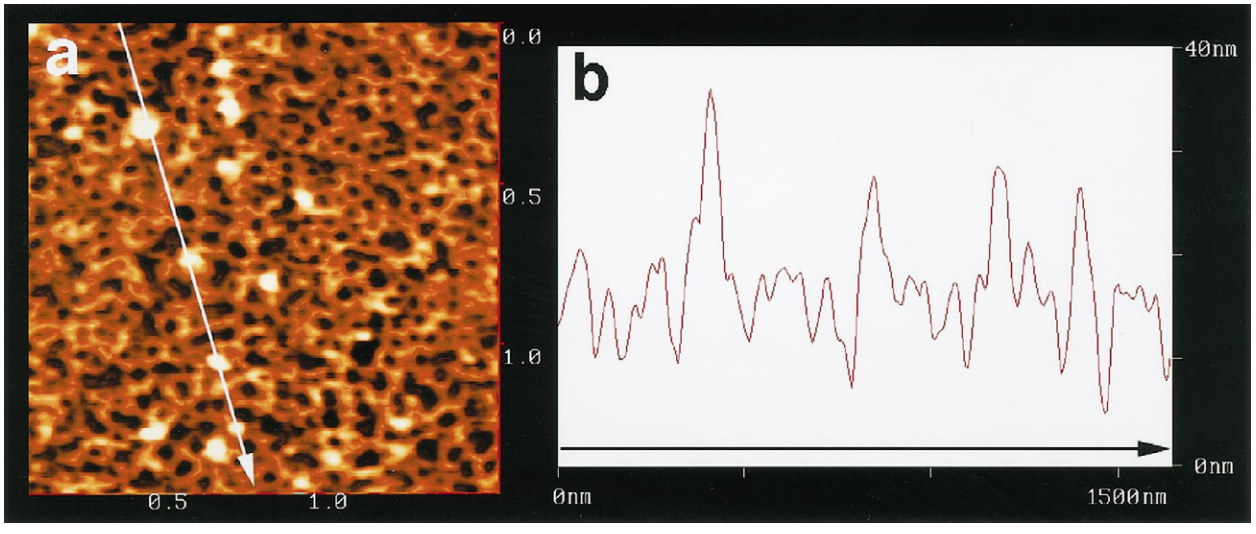

FIGURE 4 (*a*) An AFM image of a ghost labeled with 10 nm-ϕ gold particles coated with anti-spectrin antibodies. The ghost was rapidly frozen/freeze-dried (unfixed) after labeling with 10 nm-ϕ gold particles. The line indicates the place where the cross section shown in *b* was measured, and passes four particles that are likely to be gold particles. The image was processed as described in Fig. 2. Note that the height in this profile is magnified 140 times more than the lateral dimensions (scale, nm). Scales are in μm. (*b*) A representative surface contour along a line shown in *a*. The heights at the particles are ~10–20 nm, suggesting that these are 10-nm ϕ gold particles coated with anti-spectrin antibodies.

coated membrane and the partially rehydrated membrane under ambient conditions give similar images. Sharpness of the image may be slightly worse with the carbon-coated samples, which is expected for coated samples. Among the carbon-coated specimens, the order of carbon coating and rewarming (both processes and the initial freeze-drying process were performed without breaking vacuum) did not affect the results. In addition, the specimens that had been brought to ambient conditions (and thus were partially rehydrated) before carbon coating gave practically the same AFM images as the samples carbon-coated before rehydration. These results indicate that the meshwork structures seen in Figs. 2 and 3 are not due to rehydration of the ghost membrane.

Identification of the meshwork as the spectrin network

To determine whether the observed network represented the spectrin network, the following experiments were performed.

First, ghosts (unsealed) were labeled with 10-nm ϕ gold particles that had been coated with anti-spectrin antibodies. Fig. 4 *a* shows an AFM image of a ghost labeled with 10-nm ϕ gold particles. The line passes four particles that are likely to be gold particles. The surface contour along this line shown in Fig. 4 *b* indicates that the heights at these particles are 10–20 nm, suggesting that these are 10-nm ϕ gold particles coated with anti-spectrin antibodies. The average number of 10–20-nm ϕ particles per ghost is 54.0 $\pm$ 14.2 (standard error). When the gold particles were coated with

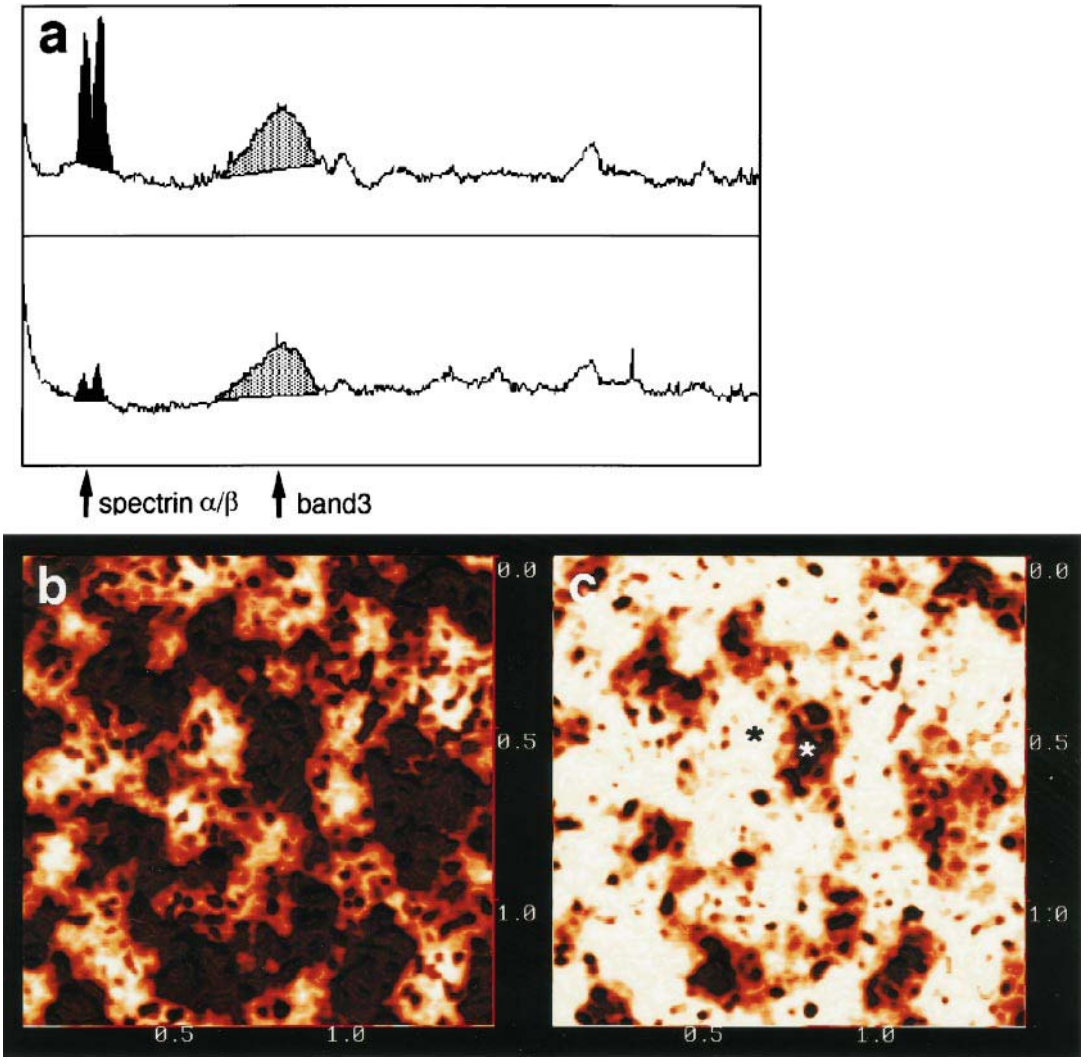

FIGURE 5 (*a*) Densitometric scan profiles of Coomassie-stained SDS polyacrylamide gel of ghosts before (*top*) and after (*bottom*) incubation in distilled water for 10 min. Water extraction of the spectrin network was carried out after the ghosts were adsorbed on a coverslip. After incubation in distilled water for 10 min, the coverslips were rapidly frozen and lyophilized. Four coverslips were treated. Two coverslips were used for AFM observation, and the remaining two coverslips were used for protein analysis by SDS-polyacrylamide gel electrophoresis. (*b* and *c*) Typical AFM images of a ghost that has been rapidly frozen/freeze-dried after incubation in distilled water for 10 min before freezing. See the text for details. The images were processed as described in Fig. 2. Scales are in μm.

control rabbit IgG, the number of 10–20-nm ϕ particles found on the surface was 10.7 ± 3.2 per ghost. Although these particles over the background of a 16-nm-thick membrane can easily be distinguished, they were not found very often in the sample when gold particles were not added. (In other figures of the ghost membrane in this paper, many particles are also visible, but they are in general much smaller (lower) than 10 nm, as seen in the surface contour in Fig. 1 *b*. Because the height in all of these images is enlarged, and because the look-up table for the height axis in these figures is shifted to enhance the contrast of the meshwork, even smaller particles hit higher bits in these displays. This is the reason why there are also many particles in other figures. These smaller particles can easily be distinguished by measuring the heights of the particles.) These results indicate that the meshwork contains spectrin.

Second, the ghosts attached to a coverslip were incubated in distilled water for 10 min to extract the spectrin meshwork from the membrane. This process greatly reduced the ratio of α/β-spectrins to band 3, an integral membrane protein, as shown by the results of sodium dodecyl sulfate-polyacrylamide gel electrophoresis (SDS-PAGE) (Fig. 5 *a*). AFM images of a ghost that had been incubated in distilled water for 10 min and then rapidly frozen and dried are shown in Fig. 5, *b* and *c*. In Fig. 5, *b* and *c*, fine structures associated with the upper and bottom membranes, respectively, are shown. These data were obtained in a single data acquisition process, but the look-up table for these displays is linearly shifted, so that fine structures of upper and bottom membranes become visible in each display. Assuming that these meshwork structures are due to the spectrin network, these images can be explained as follows. In Fig. 5 *b*, because many of the spectrin molecules had been extracted, the meshwork structure on the upper membrane covers only about half of the membrane in this particular ghost. In Fig. 5 *c*, the membrane skeleton of the lower membrane had not been much extracted in this particular ghost, and was imaged through "holes" made in the meshwork of the membrane skeleton of the upper membrane. This result, together with that in Fig. 5 *a*, suggests that the meshwork observed by AFM is indeed the spectrin network.

Based on these results, we concluded that the meshwork observed on the extracellular surface of the plasma membrane using the AFM tip represents the structure of the spectrin network on the cytoplasmic surface of the erythrocyte plasma membrane.

Optimal method for ghost preparation for AFM observations

To establish methods for observing the spectrin network of ghosts from outside the cell, we systematically examined various fixation and drying procedures. Combinations of three fixation methods (no fixation, 2% glutaraldehyde, 2% glutaraldehyde plus 0.5% osmium tetroxide) and four drying methods (rapid freezing/freeze-drying in distilled water, freeze-drying after replacing the solvent with *t*-butyl alcohol, air-drying in distilled water, and critical-point drying after replacing the solvent with ethanol) were examined. The results were compared with the published electron micrographs (Tsukita et al., 1980; Nermut, 1981; Ursitti et al., 1991; Coleman et al., 1989). The results are summarized in Table 1 and Fig. 6.

Rapid freeze/freeze-drying in water gave similar results for unfixed (Fig. 2) and glutaraldehyde-fixed (data not shown) ghosts. Air-drying of unfixed ghosts tended to result in images with a more sparse meshwork (Fig. 6 *a*). This may be due to extraction of the spectrin network during drying, which is carried out in distilled water. (For both rapid-freeze/freeze-drying and air drying, ghosts on the coverslip were rinsed in distilled water for several seconds before drying to avoid the concentration and crystallization of salts. See Materials and Methods. When samples were rapidly frozen right after rinsing, spectrin tended to stay, but when samples were dried in air, spectrin tended to be washed away because of dissociation of the network in the low-salt solution and the surface tension at the air/water interface.) Fixation with glutaraldehyde was effective for preventing the extraction of the spectrin network during air-drying, but the image obtained was less crisp and showed greater mesh sizes (Fig. 6 *b*). Freeze-drying in *t*-butyl alcohol and critical-point drying of glutaraldehyde-

TABLE 1 Summary of the results with various methods of fixation and drying

	Drying method			
Fixation method	Freeze-drying[§] from water	Air-drying[§] from water	Freeze-drying from *t*-butyl alcohol	Critical-point drying
None	Dense meshwork (Fig. 2)	Sparse meshwork (a)	Not done[¶]	Not done[¶]
Glutaraldehyde*	Dense meshwork	Less crisp (b)	Worse contrast[¶]	Worse contrast[¶]
Glutar + osmium[#]	Blurred mesh (c)	Blurred mesh	Blurred mesh	Blurred mesh

(a)–(c) indicate the corresponding AFM images shown in Fig. 6.

*Fixed with 2% glutaraldehyde.

[#]Fixed with 2% glutaraldehyde and 0.5% osmium.

[§]Samples were rinsed briefly (several seconds) in distilled water just before the drying process to avoid the concentration and crystallization of salts. The samples may be in distilled water for ~5 s or 3–10 min for freeze-drying and air-drying, respectively.

[¶]Delipidation is expected during and after the dehydration procedure for samples without osmium fixation. In the present work, samples without fixation were not used for freeze-drying in *t*-butyl alcohol or critical-point drying.

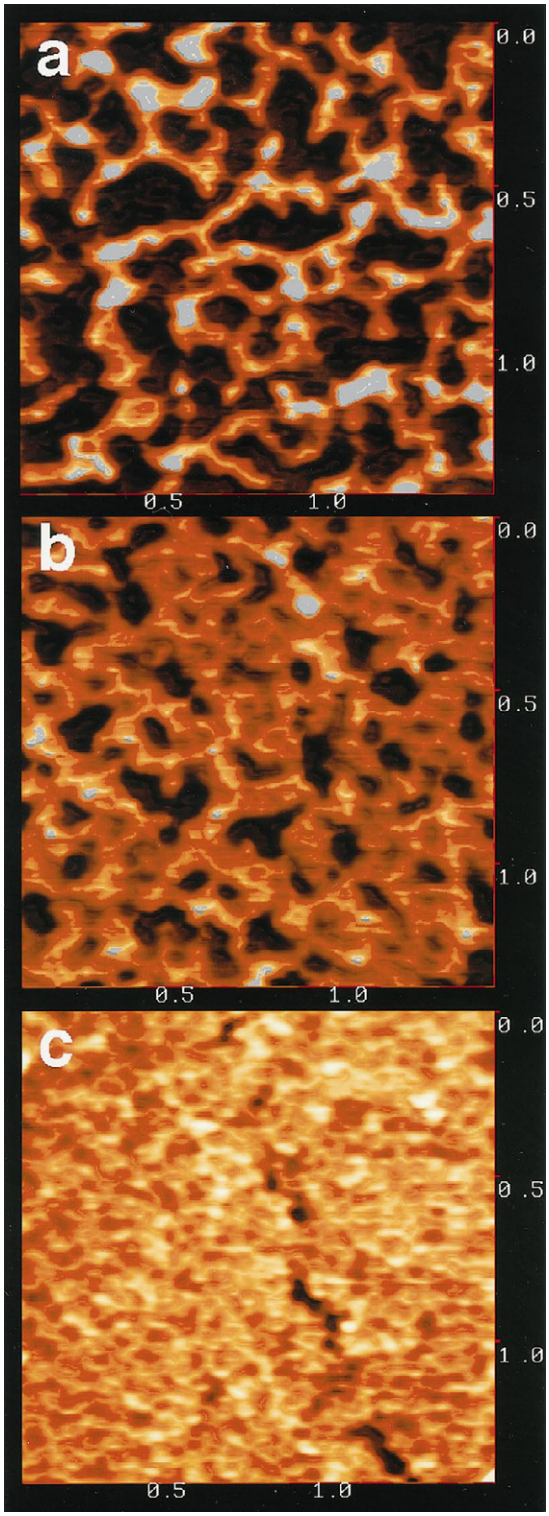

FIGURE 6 AFM images of ghosts treated with various fixation and drying procedures. Specific treatments for each sample are summarized in Table 1. These figures were processed in exactly the same way as Fig. 2. Scales are in μm.

fixed samples without postfixation with osmium tetroxide gave images with lower contrast (data not shown), but the reasons for this result are not clear. Some lipids and membrane proteins must have been extracted in the organic solvent/water phase, whereas some may be nonspecifically bound to the membrane skeleton, and this may have decreased the contrast and resolution of the image of the meshwork.

Osmium fixation (after glutaraldehyde fixation) always gave blurred images, regardless of the drying method (cf. Table 1, Fig. 6 *c*). However, the mesh size stayed the same as that before osmium fixation. This blurring effect of osmium fixation occurred even when the concentration of osmium was diluted to 0.005% (w/v). A further discussion of osmium-fixed samples is given later.

Electron micrographs by Nermut (1981) and Ursitti et al. (1991) indicate that the distances between junctions are ~60 nm on average, and that the number of junctional complexes is ~400/μm^2. These numbers suggest that the actual meshwork of the membrane skeleton is finer than the meshwork imaged here, and that the finest mesh observed here is closer to the reality. These results indicate, therefore, that the sample of rapid freeze/freeze-drying in water (but right after rinsing in water) without fixation is the best method for AFM observation of the erythrocyte membrane skeleton.

Comparison of AFM images obtained on the extracellular and the cytoplasmic surfaces of the plasma membrane

Erythrocyte ghosts were attached to a coverglass, and the part of the membrane that faced the buffer (as opposed to that which faced the coverglass) was removed by a rapid flow of buffer projected through a 25-gauge needle (lysis-squirting; Clarke et al., 1975; Nermut, 1981). The cytoplasmic surface of the membrane on the bottom could be exposed in this way (with the membrane still attached to the coverslip). Under our experimental conditions, only small fractions of ghosts on a coverslip are exposed to the fast stream of the buffer, and, in the path of the fast stream, partially blown ghosts were found only between the area of uncleaved ghosts and the area without ghosts (the area where the originally attached ghosts had been totally blown off). The sample was then rapidly frozen/freeze-dried and observed by AFM.

Fig. 7 *a* shows an AFM image of freeze-dried ghosts, in which the upper membrane had been blown off. This figure is comparable to Fig. 1 *a* for intact ghosts. The ghosts are 7–10 μm in diameter, showing that there is little lateral shrinkage of ghosts.

Fig. 7 *b* shows a representative surface contour of a ghost after lysis-squirting. Note that the vertical dimension in this profile is magnified 260 times more than the lateral dimensions. On average, the surface of the partially blasted ghost generally lies between 4 and 8 nm above the coverslip, approximately half the height of intact ghosts, indicating that these ghosts are likely to be half-ghosts. The variation in heights represents the presence of the spectrin network on the plasma membrane.

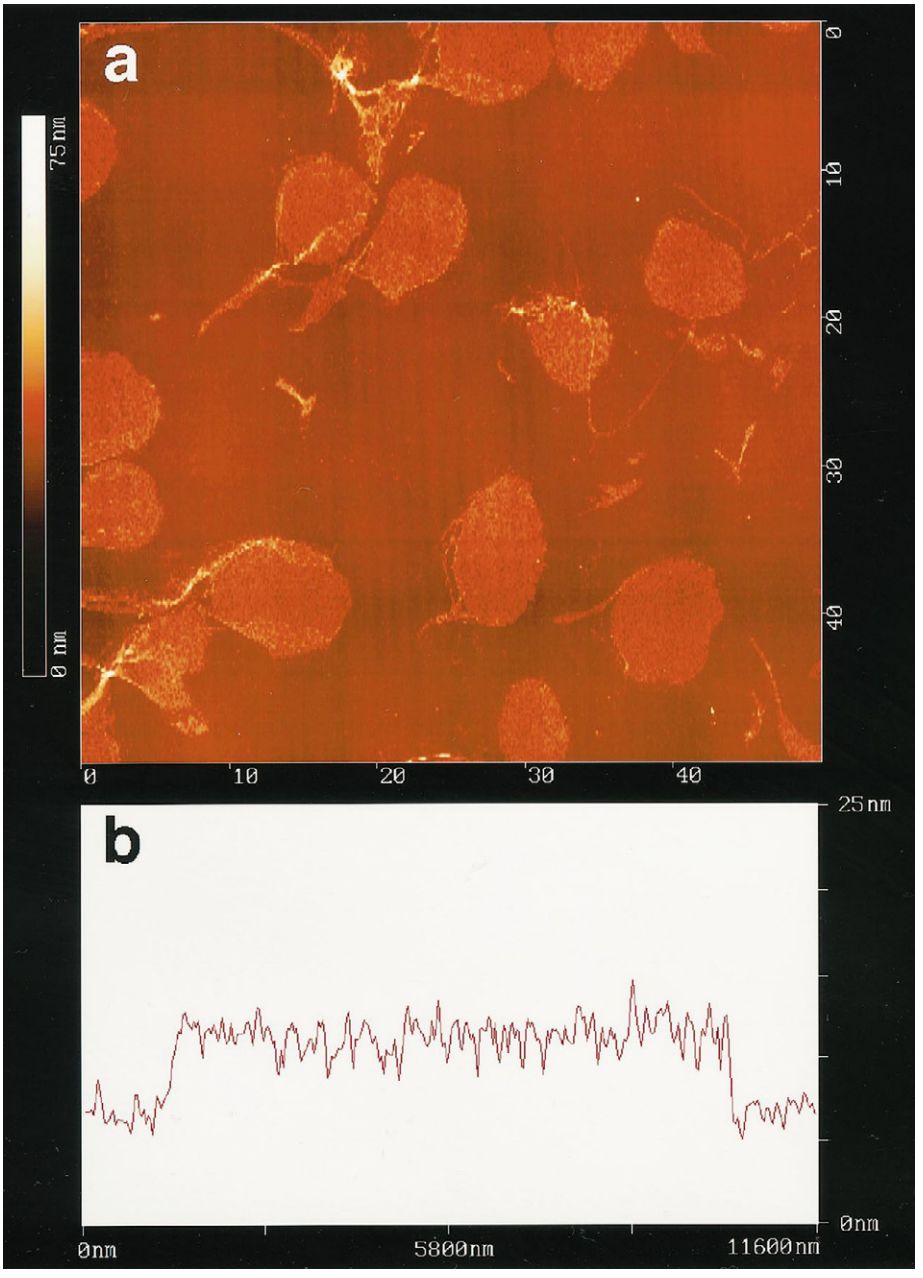

FIGURE 7 (*a*) An AFM image of rapidly frozen/freeze-dried unfixed ghosts after lysis-squirting at a low magnification. See the text for details. Scales along the side of the image are in μm. (*b*) A representative surface contour of a single ghost after lysis-squirting. Note that the height in this profile is magnified 260 times more than the lateral dimensions (scale, nm).

A representative AFM image of the cytoplasmic surface of a lysed ghost at a greater magnification is shown in Fig. 8. The meshwork was more dense than that observed on the extracellular surface of the plasma membrane (cf. Fig. 2).

The mesh sizes observed at the extracellular and the cytoplasmic surfaces of the plasma membrane were evaluated. Four representative images of 1 μm^2 for each case were selected and read into National Institutes of Health Image 1.45 software on a Macintosh personal computer, the network structure was extracted and skeletalized (Fig. 9 *a*), and the area of each mesh was measured. Distributions of the mesh area are shown in the histograms in Fig. 7 *b*. Such distributions in area may be a result of irregularities in the shape of the mesh and variations (flexibilities) in the conformation of spectrin tetramers. Unfixed and rapidly frozen/freeze-dried ghosts were used to produce these histograms. The mean areas are 3000 $\pm$ 59 and 4800 $\pm$ 140 nm^2, respectively (median values are 2540 and 3820 nm^2 for 973 and 597 meshes, respectively), as observed at the extracellular and cytoplasmic surfaces of the plasma membrane.

A junctional complex exists every 3000–5000 nm^2, as estimated from the number of spectrin tetramers in electron micrographs (Liu et al., 1987; Vertessy and Steck, 1989; McGough and Josephs, 1990). This is in general agreement with the present observation.

Mechanism of AFM imaging of the intracellular membrane skeleton on the extracellular surface of the plasma membrane

In Fig. 10 we present three possible mechanisms for AFM imaging of the intracellular membrane skeleton from the

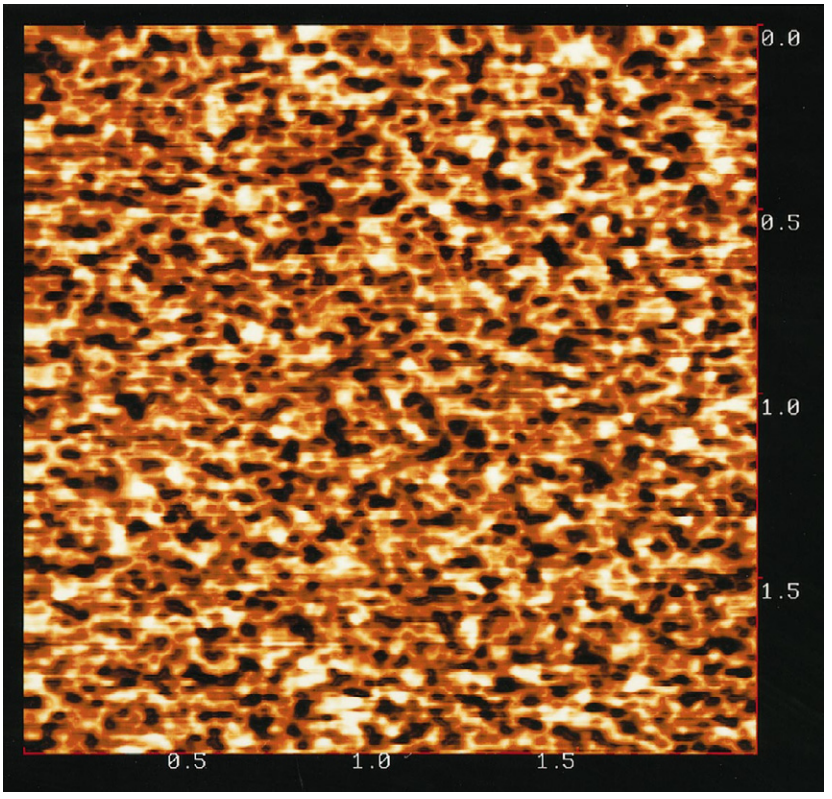

FIGURE 8 A representative high-magnification AFM image of a ghost after lysis-squirting observed on the cytoplasmic surface of the plasma membrane. The erythrocyte ghosts were adsorbed on a coverslip, and the top membrane was sheared off by a stream of buffer, which exposed the cytoplasmic surface of the membrane on the bottom. The sample was then rapidly frozen/freeze-dried and observed by AFM. The meshwork is more dense than that observed from outside the cell (cf. Fig. 2). This figure was processed in exactly the same way as Fig. 2. Scales are in μm.

extracellular surface of the cell. Scheme a assumes that with the loss of water during drying, the membrane sank inward at places where there is no support by the membrane skeleton, leaving behind the membrane skeleton and the membrane attached to it (sunken membrane model). Scheme b assumes that the membrane is depressed by the AFM tip during scanning, and that the extent of this depression is less where the membrane skeleton is present beneath the membrane (depression model). Scheme c assumes that the AFM tip penetrates the membrane, thus detecting submembranous structures such as the membrane skeleton (penetration model).

We do not think that Scheme c is likely. When we observed liposomes (data not shown) or the membrane skeleton that is associated with the lower membrane that is attached to a coverglass (lysis-squirted ghosts, Figs. 7 and 8), the tip did not penetrate to reach the glass surface, as discussed in the previous section. This result indicates that the tip does not easily penetrate the dried membrane. Bradow et al. (1993) reported that repeated scanning of the AFM tip over the lipid membrane could section the membrane, but required a force greater than 12.9 ($\pm$ 1.0) nN.

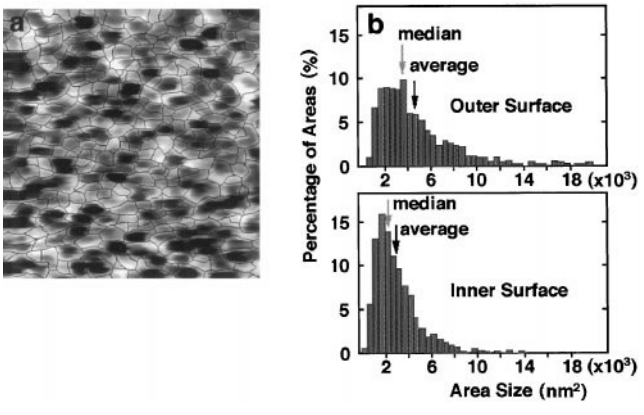

FIGURE 9 (*a*) A representative image of the skeletalized network used for measurements of individual areas bounded by the spectrin skeleton. The determined compartment boundaries are indicated in thin black lines. The size is 1 μm $\times$ 1 μm. The original AFM images were processed using National Institutes of Health Image software on a Macintosh computer, and the network structure was extracted and skeletalized. (*b*) Distributions of mesh sizes observed on the extracellular and the cytoplasmic surfaces of the plasma membrane. Three images of 1 μm^2 were randomly selected for each case.

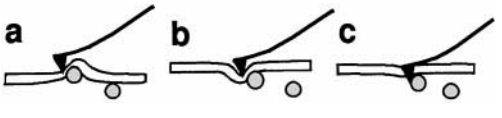

FIGURE 10 Three possible schemes for AFM imaging of the intracellular membrane skeleton from the extracellular surface of the cell. (*Scheme a*) Sunken membrane model. During drying, the membrane sinks with the loss of water into the cell where there is no support by the membrane skeleton, leaving behind the membrane skeleton and the membrane attached to it. (*Scheme b*) Depression model. The membrane is depressed by the AFM tip during scanning, and the extent of the depression is less where the membrane skeleton is present beneath the membrane. (*Scheme c*) Penetration model. The AFM tip penetrates the membrane and enters the cell, thus detecting submembranous structures such as the membrane skeleton.

The force used here was considerably less than this value (less than 3 nN).

To test Scheme a, ghosts (unfixed and freeze-dried in water) with and without carbon coating are to be compared (Figs. 3 and 2, respectively). For the carbon-coated specimen, AFM observation was carried out on top of the carbon coat. The coats with thicknesses of 2 and 3 nm were examined and gave the same results. Such carbon coats are thought to be sufficiently hard to prevent depression and/or penetration by the AFM tip. The image obtained after carbon coating is similar to that obtained without carbon coating. These results indicate that depression or penetration by the AFM tip is not necessary for imaging the membrane skeleton on the extracellular surface of the plasma membrane. Similarly, carbon-coated and uncoated specimens that had been fixed with osmium tetroxide (Figs. 11 and 6 *c*, respectively) showed practically no difference. Fig. 11 could be slightly blurrier than Fig. 6 *c*, which could be explained by the general tendency that coating decreases the image contrast.

In contrast, osmium fixation profoundly affects the image contrast, but without altering meshwork characteristics. Compare Fig. 6 *c* [osmium-fixed] with Fig. 2 [unfixed] for samples without carbon coating, and compare Fig. 11 [osmium-fixed] and Fig. 3 [unfixed] for carbon-coated specimens. Because the effect of osmium fixation on image contrast can be seen even in the carbon-coated samples, and because the extent of osmium-fixation effect is similar between carbon-coated and uncoated specimens, the osmium effect on the AFM images is likely to be intrinsic to the specimen rather than due depression or penetration of the plasma membrane by the AFM tip, i.e., the difference observed in the contrast in AFM images before and after osmium fixation is not due to changes in the extent of depression or penetration by the AFM tip, but rather to the intrinsic difference in the surface terrain between osmium-fixed and unfixed ghosts. Because osmium fixation cross-links unsaturated lipids in the membrane, it is expected that it solidifies the membrane. The solidified membranes may not sink as much as unfixed membranes when the ghosts are dried, which diminishes the contrast in AFM images of osmium-fixed cells.

These results indicate that the sunken membrane model a adequately explains why the intracellular membrane skeleton can be visualized from outside the cell.

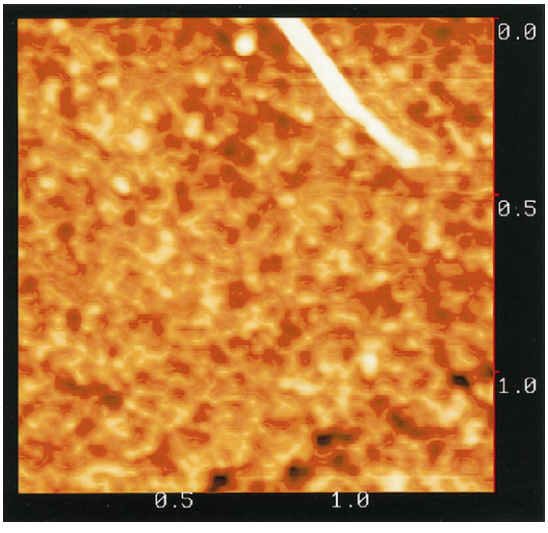

FIGURE 11 An AFM image of a carbon-coated, freeze-dried ghost after fixation with 2% glutaraldehyde and then with 0.5% osmium tetroxide. Comparison with the image of a carbon-coated unfixed ghost (Fig. 3) indicates that osmium fixation greatly reduces the image contrast. Processed in exactly the same way as Fig. 2. Scales are in μm.

DISCUSSION

In the present observation, we established methods for observing the membrane skeleton of the erythrocyte ghost at the extracellular surface of the cell that preserve the overall shape of the erythrocyte ghost. Rapid freezing by quickly immersing the coverslip into the liquid cryogen 1,1,1,2-tetrafluoroethane at −101°C (liquid/solid phase transition temperature) and subsequent lyophilization have been judged to be the best approach among those examined in the present study for preparing ghost specimens attached to a coverglass, based on the comparison with the results of rapid-freeze/deep-etch electron microscopy (Nermut, 1981; Ursitti et al., 1991). This method works well for AFM, because AFM examines the structure near the surface of the specimen, where freezing rapidly takes place. In many other AFM studies, specimens have simply been dried in the air and used for observation. The present study clearly indicates that air-drying is not suitable for preserving the intact structure of the membrane skeleton, even after glutaraldehyde fixation.

The ghost membranes were also imaged on the cytoplasmic surface, and the fine meshwork of the membrane skeleton was observed. Because the area observed on the extracellular surface is greater, and because it is likely that AFM observation on the extracellular surface characterizes the contour of the sunken membrane covering the spectrin network, it is likely that observation on the extracellular surface detects only spectrin molecules that are located close to the membrane, and that the inner part of the network could not be detected. Assuming that the shapes of the areas are similar between the images taken on the extracellular and the cytoplasmic surfaces of the plasma membrane, ~80% of the filaments (square root of 3000/4800) can be seen on the extracellular surface. The presence of a part that is unobservable from the outside indicates that the spectrin network is folded into a three-dimensional network, i.e., 20% of the skeleton may be hanging toward the inside of the cell, and the sinking membrane may not reach the parts located deep inside the cell. Observation of the membrane skeleton of erythrocytes on the extracellular and cytoplasmic surfaces of the plasma membrane may be useful in studies of the mechanism of how the membrane

skeleton supports the morphological changes of erythrocytes in the circulation, as well as how an abnormality in a component of the membrane skeleton can lead to the loss of mechanical strength and/or deformability of the erythrocyte membrane.

Experiments at the final stages in this study were carried out with an SPI 3700 AFM in Dr. Nobuo Shimamoto's laboratory at the National Institute of Genetics, where Minoru Takeuchi is currently located. Dr. Eric Henderson at BioForce Laboratory and Iowa State University, Dr. Evan A. Evans at University of British Columbia, and Mr. Michio Tomishige at the University of Tokyo provided valuable comments and suggestions.

REFERENCES

Akahori, H., H. Ishii, I. Nonaka, and H. Yoshida. 1988. A simple freeze-drying device using *t*-butyl alcohol for SEM specimens. *J. Electron Microsc.* 37:351–352.

Almqvist, N., L. Backman, and S. Fredriksson. 1994. Imaging human erythrocyte spectrin with atomic force microscopy. *Micron.* 25:227–232.

Beaven, G. H., L. Jean-Baptiste, E. Ungewickell, A. J. Baines, F. Shahbakhti, J. C. Pinder, S. E. Lux, and W. B. Gratzer. 1985. An examination of the soluble oligomeric complexes extracted from the red cell membrane and their relation to the membrane cytoskeleton. *Eur. J. Cell Biol.* 36:299–306.

Bennett, V. 1990. Spectrin-based membrane skeleton: a multipotential adaptor between plasma membrane and cytoplasm. *Physiol. Rev.* 70: 1029–1065.

Bennett, V., and D. M. Gilligan. 1993. The spectrin-based membrane skeleton and micron-scale organization of the plasma membrane. *Annu. Rev. Cell Biol.* 9:27–66.

Boal, D. H. 1994. Computer simulation of a model network for the erythrocyte cytoskeleton. *Biophys. J.* 67:521–529.

Boal, D. H., and S. K. Boey. 1995. Barrier-free paths of directed protein motion in the erythrocyte plasma membrane. *Biophys. J.* 69:372–379.

Bradow, S. L., D. C. Turner, B. R. Ratna, and B. P. Gaber. 1993. Modification of supported lipid membranes by atomic force microscopy. *Biophys. J.* 64:898–902.

Butt, H. J., E. K. Wolff, S. A. C. Gould, B. D. Northern, C. M. Peterson, and P. K. Hansma. 1990. Imaging cells with the atomic force microscope. *J. Struct. Biol.* 105:54–61

Byers, T. J., and D. Branton. 1985. Visualization of the protein associations in the erythrocyte membrane skeleton. *Proc. Natl. Acad. Sci. USA.* 82:6153–6157.

Chang, L., T. Kious, M. Yorgancioglu, D. Keller, and J. Pfeiffer. 1993. Cytoskeleton of living, unstained cells imaged by scanning force microscopy. *Biophys. J.* 64:1282–1286.

Clarke, M., G. Schatten, D. Mazia, and J. A. Spudich. 1975. Visualization of actin fibers associated with the cell membrane in amoebae of *Dictyostelium discoideum. Proc. Natl. Acad. Sci. USA.* 72:1758–1762.

Coleman, T. R., D. J. Fishkind, M. S. Mooseker, and J. S. Morrow. 1989. Functional diversity among spectrin isoforms. *Cell Motil. Cytoskel.* 12:225–247.

Costello, M. J. 1980. Ultra-rapid freezing of thin biological samples. *Scan. Electron Microsc.* 1980/II:361–370.

Elder, H. Y., C. C. Gray, A. G. Jardine, J. N. Chapman, and W. H. Biddlecombe. 1982. Optimum condition for cryoquenching of small tissue blocks in liquid coolants. *J. Microsc.* 126:45–61.

Evans, E. A. 1989. Structure and deformation properties of red blood cells: concepts and quantitative methods. *Methods Enzymol.* 173:3–35.

Gilligan, D. M., and V. Bennett. 1993. The junctional complex of the membrane skeleton. *Semin. Hematol.* 30:74–83.

Gould, S. A. C., B. Drake, C. B. Prater, A. L. Wesienhorn, S. Manne, H. G. Hansma, P. K. Hansma, J. Massie, M. Longmire, V. Elings, B. Dixon Northern, B. Mukergee, C. M. Peterson, W. Stoeckenius, T. R. Albrecht, and C. F. Quate. 1990. From atoms to integrated circuit chips, blood cells, and bacteria with the atomic force microscope. *J. Vac. Sci. Technol.* A8:369–373.

Hainfeld, J. F., and T. L. Steck. 1977. The sub-membrane reticulum of the human erythrocyte: a scanning electron microscope study. *J. Supramol. Struct.* 6:301–311.

Hammerton, R. W., K. A. Krzeminski, R. W. Mays, T. A. Ryan, D. A. Wollner, and W. J. Nelson. 1991. Mechanism for regulating cell surface distribution of Na^+,K^+-ATPase in polarized epithelial cells. *Science.* 254:847–850.

Han, W., J. Mou, J. Sheng, J. Yang, and Z. Shao. 1995. Cryo atomic force microscopy: a new approach for biological imaging at high resolution. *Biochemistry.* 34:8215–8220.

Henderson, E., P. G. Haydon, and D. S. Sakaguchi. 1992. Actin filament dynamics in living glial cells imaged by atomic force microscopy. *Science.* 257:1944–1946.

Hitt, A. T., and E. J. Luna. 1994. Membrane interactions with the actin cytoskeleton. *Curr. Opin. Cell Biol.* 6:120–130.

Horber, J. K., J. Mosbacher, W. Haberle, J. P. Ruppersberg, and B. Sakmann. 1995. A look at membrane patches with a scanning force microscope. *Biophys. J.* 68:1687–1693.

Inoue, T., and H. Osatake. 1988. A new drying method of biological specimens for scanning electron microscopy: the *t*-butyl alcohol freeze-drying method. *Arch. Histol. Cytol.* 51:53–59.

Inoue, T., H. Osatake, and H. Takahashi. 1989. A new freeze-drying instrument using *t*-butyl alcohol for scanning electron microscopy. *J. Electron Microsc.* 38:246–249.

Jacobson, K., E. D. Sheets, and R. Simon. 1995. Revisiting the fluid mosaic model of membranes. *Science.* 268:1441–1442.

Kusumi, A., and Y. Sako. 1996. Cell surface organization by the membrane skeleton. *Curr. Opin. Cell Biol.* 8:566–574.

Lal, R., B. Drake, D. Blumberg, D. R. Saner, P. K. Hansma, and S. C. Feinstein. 1995. Imaging real-time neurite outgrowth and cytoskeletal reorganization with an atomic force microscope. *Am. J. Physiol.* 269: C275–C285.

Leunissen, J. L. M., and J. R. De May. 1989. Preparation of gold probes. *In* Immunogold Labeling in Cell Biology. A. J. Verkleij and J. L. M. Leunissen, editors. CRC Press, Boca Raton, FL. 3–16.

Liu, S. C., L. H. Derick, and J. Palek. 1987. Visualization of the hexagonal lattice in the erythrocyte membrane skeleton. *J. Cell Biol.* 104:527–536.

Liu, S. C., P. Windisch, S. Kim, and J. Palek. 1984. Oligomeric states of spectrin in normal erythrocyte membranes: biochemical and electron microscopic studies. *Cell.* 37:587–594.

Luna, E. J., and A. L. Hitt. 1992. Cytoskeleton-plasma membrane interactions. *Science.* 258:955–964.

Lux, S. E. 1979. Dissecting the red cell membrane skeleton. *Nature.* 281:426–428.

Marchesi, V. T. 1985. Stabilizing infrastructure of cell membranes. *Annu. Rev. Cell. Biol.* 1:531–561.

McGough, A. M., and R. Josephs. 1990. On the structure of erythrocyte spectrin in partially expanded membrane skeletons. *Proc. Natl. Acad. Sci. USA.* 87:5208–5212.

Mohandas, N., and J. A. Chasis. 1993. Red blood cell deformability, membrane material properties and shape: regulation by transmembrane, skeletal and cytosolic proteins and lipids. *Semin. Hematol.* 3:171–192.

Nermut, M. V. 1981. Visualization of the "membrane skeleton" in human erythrocytes by freeze-etching. *Eur. J. Cell Biol.* 25:265–271.

Ohanian, V., L. C. Wolfe, K. M. John, J. C. Pinder, S. E. Lux, and W. B. Gratzer. 1984. Analysis of the ternary interaction of the red cell membrane skeletal proteins spectrin, actin, and 4.1. *Biochemistry.* 23: 4416–4420.

Pietrasanta, L. I., A. Schaper, and T. M. Jovin. 1994. Imaging subcellular structures of rat mammary carcinoma cells by scanning force microscopy. *J. Cell Sci.* 107:2427–2437.

Rutter, G., and H. Hohenberg. 1991. Simultaneous demonstration of antigens on outer and protoplasmic surfaces of the plasma membrane by replica immunocytochemistry. *In* Colloidal Gold, Vol. 3. Principles, Methods, and Applications. M. A. Hayat, editor. Academic Press, New York. 151–186.

Sako, Y., and A. Kusumi. 1994. Compartmentalized structure of the plasma membrane for receptor movements as revealed by a nanometer-level motion analysis. *J. Cell Biol.* 125:1251–1264.

Sako, Y., and A. Kusumi. 1995. Barriers for lateral diffusion of transferrin receptor in the plasma membrane as characterized by receptor dragging by laser tweezers: fence versus tether. *J. Cell Biol.* 129:1559–1574.

Sheets, E. D., R. Simson, and K. Jacobson. 1995. New insights into membrane dynamics from the analysis of cell surface interactions by physical methods. *Curr. Opin. Cell Biol.* 7:707–714.

Sheetz, M. P., and D. Sawyer. 1978. Triton shells of intact erythrocytes. *J. Supramol. Struct.* 8:399–412.

Sheetz, M. P., M. Schindler, and D. E. Koppel. 1980. Lateral mobility of integral membrane proteins is increased in spherocytic erythrocytes. *Nature.* 285:510–512.

Shen, B. W., R. Josephs, and T. L. Steck. 1986. Ultrastructure of the intact skeleton of the human erythrocyte membrane. *J. Cell Biol.* 102: 997–1006.

Shotton, D. M., B. E. Burke, and D. Branton. 1979. The molecular structure of human erythrocyte spectrin. *J. Mol. Biol.* 131:303–329.

Sommer, J. R. 1977. To cationize glass. *J. Cell Biol.* 75:245a.

Timme, A. H. 1981. The ultrastructure of the erythrocyte cytoskeleton at neutral and reduced pH. *J. Ultrastruct. Res.* 77:199–209.

Tsuji, A., K. Kawasaki, and S. Ohnishi. 1988. Regulation of band 3 mobilities in erythrocyte ghost membranes by protein association and cytoskeletal meshwork. *Biochemistry.* 27:7447–7452.

Tsukita, Sa., Sh. Tsukita, and H. Ishikawa. 1980. Cytoskeletal network underlying the human erythrocyte membrane. *J. Cell Biol.* 85:567–576.

Tsukita, Sh., Sa. Tsukita, A. Nagafuchi, and S. Yonemura. 1992. Molecular linkage between cadherins and actin filaments in cell-cell adherens junctions. *Curr. Opin. Cell Biol.* 4:834–839.

Ursitti, J. A., D. W. Pumplin, J. B. Wade, and R. J. Bloch. 1991. Ultrastructure of the human erythrocyte cytoskeleton and its attachment to the membrane. *Cell Motil. Cytoskel.* 19:227–243.

Ursitti, J. A., and J. B. Wade. 1993. Ultrastructure and immunocytochemistry of the isolated human erythrocyte membrane skeleton. *Cell Motil. Cytoskel.* 25:30–42.

Vertessy, B. G., and T. L. Steck. 1989. Elasticity of the human red cell membrane skeleton. *Biophys. J.* 55:255–262.

Weinstein, R. S., H. D. Tazelaar, and J. M. Loew. 1986. Red cell comets: ultrastructure of axial elongation of the membrane skeleton. Reply to commentary. *Blood Cells.* 11:363–366.

Zhang, Y., S. J. Sheng, and Z. Shao. 1996. Imaging biological structure with the cryo atomic force microscope. *Biophys. J.* 71:2168–2176.